PREPRINT UCRL-77640

CONF-760708--2

Lawrence Livermore Laboratory

Computation Of Mach Reflection From Rigid And Yielding Surfaces

Alfred C. Buckingham and Sharon S. Wilson

Paper No. 76-324
AIAA 9th Fluid and Plasma Dynamics
Conference San Diego, California / July 14-16, 1976

COMPUTATION OF MACH REFLECTION FROM RIGID AND YIELDING SURFACES[+]

Alfred C. Buckingham[*] and Sharon S. Wilson[**]
Lawrence Livermore Laboratory
University of California
Livermore, California

ABSTRACT

The present discussion centers on a theoretical description of one aspect of the irregular or Mach reflection from solid surfaces. The discussion is restricted to analytical considerations and some preliminary results using model approximations to the surface interaction phenomena. Currently, full numerical simulations of the irregular reflection surface interaction dynamics have not been obtained since the method is still under development. Discussion of the numerical method is, therefore, restricted to some special procedures we intend to implement for the gas-solid surface boundary dynamics. The discussion is divided into an introductory section briefly describing a particular Mach reflection process we are studying. Subsequently, we submit some of the considerations on boundary conditions for numerical treatment of the gas-solid interface. Analysis and discussion of a yielding solid surface subjected to impulsive loading from an intense gas shock wave follows. This is used as a guide for the development of the numerical procedure. Mach reflection processes are then briefly reviewed with special attention for similitude and singular perturbation features. Ultimately, the direction of our future investgations is indicated.

[+]Worked performed under the auspices of the U.S. Energy Research & Development Administration, Contract No. W-7405-Eng-48.

[*]Physicist, H-Division, LLL

[**]Mathematician, H-Division, LLL

I. INTRODUCTION

This discussion addresses two distinct but related topics. The major portion of our work to date has been directed to the dynamical interaction of a yielding solid which has been impulsively shock-loaded by a gas. Most of our preliminary analysis and discussion emphasizes simulation and analysis of this dynamic coupling process. Momentum and energy exchange and transport are the focus with special attention to irreversible processes that develop and subsequently weaken the gas shock intensity during interaction.

The briefest portion of the work to date concerns the structure of the Mach reflection itself. The investigation is directed towards fluid mechanical features of the triple point and slip line contact with the surface. Hence, this study is oriented differently from that of the cited USSR studies which emphasize non-ideal gas state behavior[1,2,3].

The current work is in its early stage. The present discussion is, therefore, purposely limited to preliminary theoretical analysis. Our attention is on both single and double Mach reflection of intense, shock-tube generated shock waves reflecting from planar wedge surfaces. The experimental studies of Gvozdeva, et. al.[1,2] are used to illustrate the physical process. In addition, the extensive experimental data base provided by Zaslavskii and Safarov[3] is examined for similitude features.

The shock wave configuration in the physical plane during single and double Mach reflections are sketched in Figs. 1 and 2, respectively. In these figures, we denote the incident shock (I), reflected shock (R), Mach stem (S), and the slip line (D). The slip line separates the singly

shocked gas processed by the Mach stem from the double shocked gas processed by the incident and reflected waves. This slip line is a demarcation between different entropy states of the gas. Pressure equilibration is maintained to either side of the slip line in accordance with the known conditions for contact discontinuities.

Experiments[1,2] reveal that the flow behind the Mach stem, which contacts the surface normally, is tangent to the wedge surface upstream of the slip line but stagnates against the wedge surface. Stagnation of significant normal velocity component occurs just downstream of the slip line. A second pressure peak results which is generally higher than that associated with the Mach stem contact point. At higher shock intensities, the slip line contact point is moved forward towards the Mach stem by this second high pressure peak. As shock intensity increases, the Mach stem distorts and an inflection may occur in the reflected shock (see Figure 2). This inflection appears to be the site of incipent formation of a second Mach stem. Sufficiently high shock intensities reproducibly generate the double Mach stem structure[1,2].

II. YIELDING SURFACE ANALYSIS

Boundary Conditions

The elastic-plastic yielding of a solid surface intensely loaded by a gas dynamic shock wave alters the gas flow in contact by its motion. The outline here is directed to development of a new, accurate, and computationally efficient method to simulate the coupled gas-solid dynamic response. A particular incentive here is the challenge to be able to predict both bounding surface response and the modification to interior pressure waves when the bounding solid surface yields. Our discussion here is limited to two-dimensional unsteady inviscid flow in the immediate neighborhood of an impermeable yielding solid surface. The restrictive, adiabatic, stream surface relations for flow in parallel contact with the surface are invoked. The governing gas dynamic equations useful for our discussion are written in x, y cartesian coordinates.

Continuity

$$\frac{\partial \rho}{\partial t} + \frac{\partial(\rho u)}{\partial x} + \frac{\partial(\rho v)}{\partial y} = 0, \tag{1}$$

X Momentum

$$\frac{\partial \rho u}{\partial t} + \rho u\frac{\partial u}{\partial x} + \rho v\frac{\partial u}{\partial y} + \frac{\partial p}{\partial x} = 0, \tag{2}$$

Y Momentum

$$\frac{\partial \rho v}{\partial t} + \rho u\frac{\partial v}{\partial x} + \rho v\frac{\partial v}{\partial y} + \frac{\partial p}{\partial y} = 0, \tag{3}$$

State

$$p = p(\rho, e), \tag{4}$$

Adiabatic Stream Surface

$$\frac{\partial \bar{S}}{\partial t} + u\frac{\partial \bar{S}}{\partial x} + v\frac{\partial \bar{S}}{\partial y} = 0. \tag{5}$$

Here the velocity components, $\vec{U} = u\vec{i} + v\vec{j}$, are aligned with the cartesian directions $\vec{r} = x\vec{i} + y\vec{j}$, respectively. For illustration, Figure 3 outlines the two cases of gas dynamic-solid boundary interaction of interest here. The top of the figure depicts a fluid to full constitutive strength solid interaction which we discuss further here. The bottom figure, the moving contact discontinuity, is the subject of a more general discussion which is deferred for a later publication.

The boundary condition treatment follows Kentzer's[4] use of the matching of characteristic surfaces in a plane parallel to the moving solid boundary. Our particular emphasis on characteristic surfaces derives from the useful concept that only such surfaces in a hyperbolic flow domain admit discontinuous derivatives. The boundary conditions on the yielding solid surface are sought in the partial derivative form of the dependent (field) variables. Development of a more accurate discrete approximation for these partial derivative boundary conditions as opposed to the variables themselves is possible since the boundary conditions are linear in the parital derivatives.

Consider, the upper sketch in Figure 3 in which we define the normal, $\vec{n}$ to the yielding surface (shown cross-hatched) which forms an angle of slope, $\frac{dy}{dx}$, with respect to the x,y cartesian plane coordinates indicated. Angular increment is measured anti-clockwise from the positive x axis. In the figure, the solid region stress tensor designated by the crossed arrows is denoted, Σ_{ij} (time). The solid region solutions are assumed known at discrete time intervals from a separate but connected solution of the continuum full strength (Lagrangian) solid domain. Outward characteristics emanating from the solid surface at points i and i-1 are

denoted C_i and C_{i-1}. $\dot{S}$ is the surface velocity.

In accordance with Kentzer's[4] procedure, matching of two characteristic surfaces is prescribed for the boundary condition development. The surfaces "wet" the yielding solid and, therefore, are normal to $\vec{n}$, the unit outward normal vector drawn from the surface S. The yielding surface motion over the interval [t, t+dt] is depicted in the figure which shows the surface subjected to impulsive shock loading.

The compatibility condition for the wave surface component flow is written[4] in our geometry:

$$\frac{\partial p}{\partial t} + \left(u+c\,\frac{dx}{ds}\right)\frac{\partial p}{\partial x} + \left(v+c\,\frac{dy}{ds}\right)\frac{\partial p}{\partial y} + \rho c\left(\frac{\partial u}{\partial t}\frac{dx}{ds} + \left(u\,\frac{dx}{ds} + c\right)\frac{\partial u}{\partial x} + v\frac{\partial u}{\partial y}\frac{dx}{ds}\right)$$

$$+ \rho c\left(\frac{\partial v}{\partial t}\frac{dy}{ds} + u\frac{\partial v}{\partial x}\frac{dy}{ds} + \left(v\frac{dy}{ds} + c\right)\frac{\partial v}{\partial y}\right) \qquad (6)$$

The isentropic condition on the stream surface characteristic is written by combining Eqs. (2) and (3) with the entropy conservation Eq. (5) and the entropy-sound speed relations

$$\frac{\partial p}{\partial x} = c^2\frac{\partial \rho}{\partial x} + \frac{\partial p(\rho,\tilde{S})}{\partial \tilde{S}}\,\frac{\partial \tilde{S}}{\partial x}\,,$$

$$\frac{\partial p}{\partial y} = c^2\frac{\partial \rho}{\partial y} + \frac{\partial p(\rho,\tilde{S})}{\partial \tilde{S}}\,\frac{\partial \tilde{S}}{\partial y}\,, \qquad (7)$$

This gives the adiabatic stream surface characteristic equation,

$$c^2\left(\frac{\partial \rho}{\partial t} + u\frac{\partial \rho}{\partial x} + v\frac{\partial \rho}{\partial y}\right) - \left(\frac{\partial p}{\partial t} + u\frac{\partial p}{\partial x} + v\frac{\partial p}{\partial y}\right) = 0. \tag{8}$$

Projection of the streamwise momentum equation to the particle-stream surface characteristic obtains

$$\left(\frac{\partial \rho u}{\partial t} + \rho u \frac{\partial u}{\partial x} + \rho v \frac{\partial u}{\partial y}\right)\frac{dy}{ds} - \left(\frac{\partial \rho v}{\partial t} + \rho u \frac{\partial v}{\partial x} + \rho v \frac{\partial v}{\partial y}\right)\frac{dx}{ds} + \left(\frac{\partial p}{\partial x}\frac{dy}{ds} - \frac{\partial p}{\partial y}\frac{dx}{ds}\right) = 0. \tag{9}$$

The directional components x,y are as shown in Figure 3, while

$$ds^2 = dx^2 + dy^2,\ x' = \frac{dx}{ds},\ y' = \frac{dy}{ds}.$$

For the yielding impermeable wall, the dynamic boundary condition is written in terms of the instantaneous wall velocity, $\dot{\xi}$

$$(BC)_A = \vec{n}\cdot\vec{U} - \dot{\xi} = u\frac{dx}{ds} + v\frac{dy}{ds} - \dot{\xi} = 0. \tag{10}$$

The general kinematic condition, Eq. (10), for solid-to-gas interface motion applies to both sides of the boundary in the absence of a solid domain. This situation corresponds to the moving contact discontinuity,

about which more will be discussed in a subsequent publication. Here we limit our remarks to the comment that in the contact discontinuity situation, Eq. (10), provides an additional surface boundary condition with the signs on the right hand side reversed when applied to the downstream side.

The procedure outlined thus far closely parallels Kentzer's[4] very interesting technique for treating impermeable moving wall boundary conditions. At this point, however, we find it advantageous to take advantage of a simple wave correction procedure in the matching of stream surface and wave surface conditions at the solid-gas interface. For a better perspective, it is useful to recall that a numerically exact matching of the general method-of-characteristics at a solid boundary requires a substantial amount of iteration. This is particularly cumbersome where transients are present, since the characteristic paths change with time. For practicality and efficiency, we shall avoid the added complexity of the characteristics iteration in our procedure. As Abbett[5] pointed out, the accuracy achieved using Kentzer's [4] method, derives, in part, from the effectiveness in the use of partial derivative boundary conditions matching characteristic and surface streamlines. Kentzer's method, however, avoids the use of the tedious method-of-characteristic iteration.

In regions of strong compressions, Kentzer's method compares well with the numerically exact method-of-characteristics computations for stationary flow[5]. However, in expanding flow, the results while good, are no longer of the same order of accuracy as that of the method-of-characteristics, no Abbett's[5] simple wave corrector scheme. This latter method makes use of infinitesimal simple wave flow change approximations in conjunction with a corrector step in the explicit MacCormack[6] predictor-corrector method. In our present approach,

we attempt to combine the Kentzer and Abbett methods with a view to extending the combined methods to non-steady fluid-solid interactive boundary problems.

The solution for the Lagrangian region[10] proceeds separately from the Eulerian (gas dynamic) region. It contains strength, constitutive strain and strain-rate information which is automatically converted to volumetric deformations and displacements at the boundary for each incremental cycle of time integration. The solid continuum eliminates the need for applying Eq. (10) in its determination. Instead, its presence is used to fulfill exactly Eq. (10) and to supply to the Eulerian region the forcing function associated with the solid strain rate and acceleration history. The needed surface motion, $\dot{S}$, geometry and directional cosines are, thereby, available from the solid region computation. On the gas dynamic side, Eq. (10) is used to inter-relate the two components of gas motion at the surface with the surface motion. A time derivative of Eq. (10) is combined with a time derivative of the surface geometry changes. The equation, together with the adiabatic stream surface condition, Eq. (8), the momentum equation, Eq. (9), and the compatibility conditions for the wave surface (6), rewritten in terms of the directional surface derivatives supply the four differential boundary conditions associated with the four unknowns: u, v, ρ, p at the surface.

The set of partial derivative boundary conditions are developed for our geometry, Figure 3. Cross differentiation, combination, and some geometric subscitutions result in:

$$\frac{\partial \rho}{\partial t} = \left(\frac{1}{c^2}\right)\left(u \frac{\partial p}{\partial x} + v \frac{\partial p}{\partial y} + \frac{\partial p}{\partial t}\right) - \left(u \frac{\partial \rho}{\partial x} + v \frac{\partial \rho}{\partial y}\right), \qquad (11)$$

$$\frac{\partial p}{\partial t} = -\rho c \left\{ \left(\frac{u}{c} + x'\right)\frac{1}{\rho}\frac{\partial p}{\partial x} + \left(\frac{v}{c} + y'\right)\frac{1}{\rho}\frac{\partial p}{\partial y} + \left[(c + ux')\frac{\partial u}{\partial x} + (c + vy')\frac{\partial v}{\partial y} \right.\right.$$

$$\left.\left. + \left(v\frac{\partial u}{\partial y}x' + u\frac{\partial v}{\partial x}y'\right] + B(S)\right\}, \right. \tag{12}$$

$$\frac{\partial u}{\partial t} = y' D(u,v,p) + B(S)x', \tag{13}$$

$$\frac{\partial v}{\partial t} = x' D(u,v,p) + B(S)y', \tag{14}$$

where,

$$B(S) = \frac{\partial(y'/x')}{\partial t}(uy' - vx') - \frac{\dot{S}R}{xx' + yy'}\left\{\left(\frac{x}{R}\right)\left(x'\frac{\partial u}{\partial x} + y'\frac{\partial v}{\partial x}\right)\right.$$

$$\left. + \left(\frac{y}{R}\right)\left(x'\frac{\partial u}{\partial y} + y'\frac{\partial v}{\partial y}\right)\right\} + \dot{S},$$

$$D(u,v,p) = u\left(\frac{\partial u}{\partial x}y' + \frac{\partial v}{\partial x}x'\right) + v\left(\frac{\partial u}{\partial y}y' + \frac{\partial v}{\partial y}x'\right) + \frac{1}{\rho}\left(\frac{\partial p}{\partial x}y' + \frac{\partial p}{\partial y}x'\right),$$

$$R = (x^2 + y^2)^{\frac{1}{2}},$$

$$(\dot{}) \equiv \frac{d(\ )}{dt}\ ,\ (\ddot{}) \equiv \frac{d^2(\ )}{dt^2}\ .$$

The procedure is outlined in steps in Figure 4. Familiarity with MacCormack's[6] four-step space and time split, second order finite difference scheme is assumed. Adjacent to a moving boundary, the four-step predictor-corrector sequence is modified as shown.

Suppose we are updating the flow properties at the cell-centered points ("X_L") indicated by the heavy arrow. Our time flow is from left to right in the diagram. Consider that step (1)$^{N+1}$ and (2)$^{N+1}$ have been completed, updating point "X_{L-1}" on the left. The step (2)$^{N+1}$ may be considered a y sweep predictor, L(y) for updating "X_L". This is followed by step (3), a one-sided L(x) predictor connecting "X_{L-1}" with "X_L" and setting tentative values of u,v,ρ,p at "X_L". In supersonic flow, the corrector sweep, L(x), is replaced by numerical integration of the governing surface flow equations: Eqns. (11), (12), (13), and (14), which are valid everywhere is supersonic flow, provided that the surface itself is not aligned with the characteristics.

In subsonic flow, the ordinary L(x) corrector sweep is restored for the point "X_L". However, this sweep is over the surface, step (4) instead of the off-surface line, step (3) used in the predictor. A coupling of the tangential surface distribution of flow properties is then established in "correcting" the values at "X_L" through a normal (but one-sided) finite difference corrector step (5). Alternatively, for flows in which the characteristic path, represented by a forward facing simple wave emanating from the surface, intersects the point "x_L", the "corrector" step (5) is replaced by a simple wave correction to the flow distribution which is constant along the path of the simple wave (shown dashed).

In the interval, over the surface spatial segment, ΔL, between the two interpolated boundary points (shown as open circular symbols in Figure 4) the infinitesimal change in surface slope on the characteristic paths is expressed as the unsteady directional partial derivatives:

$$\frac{\partial x}{\partial t} = \frac{\partial f}{\partial t} - \Delta L \frac{\partial \omega}{\partial t} \cos \omega - \frac{\partial (\Delta L)}{\partial t} \sin \omega,$$

$$\frac{\partial Y}{\partial t} = \frac{\partial g}{\partial t} - \Delta L \frac{\partial \omega}{\partial t} \sin \omega + \frac{\partial (\Delta L)}{\partial t} \cos \omega. \qquad (15)$$

In Eq. (15), f and g are spatial distribution functions representing the non-uniform variation of the flow properties over a sequence of non-centered simple waves (for centered simple waves f, g = 0). The angle, ω, is the clockwise angular displacement of the characteristic from the positive y axis in our geometry. Solutions of Eqs. (11) through (14) over step (4) give us the incremental changes over the whole surface interval, ΔL. It remains to describe the variation (in time) of the simple wave properties connecting "X_L" with the surface at a point intermediate to ΔL, as shown in Figure 4. Simple wave incremental expansions of the variables u,v,ρ,p, truncated at second order for this surface interval, $\Delta \ell < \Delta L$ are used to give us a set of algebraic incremental changes associated with this sub interval. The simple wave expansions are matched to the distribution known from solutions of Eqs. (11) through (14) on the surface. The properties are then determined at the point of intersection as well as the initial slope of the characteristic surface from Eq. (15). The properties at point "X_L" are now "updated" using the MacCormack corrector step, but conceptually along the dashed characteristic path in place of (5).

While the use of the simple wave correction is itself an elementary change in the formulation, its implementation with arbitrary geometrical surface orientations, partially covered Eulerian finite difference meshes, mixed flow regions, and unsteady changes in both variables and geometry, removes it from the realms of trivial tasks. It remains one of the primary logical programming problems we have to overcome.

Energy Response

Here we offer a few remarks and results on the effects of Solid surface dilation and linear strain rate following impulsive shock wave loading from an adjacent gas phase to solid interaction. We describe the results of a model analysis which applies a Hertzian vibrational yield to the contact surface between gas and solid. These are matched to characteristic expansions with the gas phase at the surface interface. The expansions and the modeled independent variables incorporate a single spatial dimension in the primary or vector impact direction together with time which is transformed into Fourier component response. The model is linear and, thereby, admits a relatively primitive characterization of the wave interaction at the impulsively loaded solid surface. Further discussion of the model will be outlined during the conference. At present, we defer further characterization of the model, its effectiveness, and development until a more complete data base is available from the forthcoming general numerical simulations.

Initially, the question we attempt to answer pertains to a description of the instantaneous energy and momentum coupling between the shocked gas and the solid surface. Is it possible to characterize and assess not only the partition of energy and momentum between gas and solid, but also the rate of transfer?

Figure 5 shows the geometry in which we first demonstrated both the effectiveness and the necessity of the model procedure to approximate the near-surface derivatives of energy and stress absorbed by a target solid following shock impulsive loading by hypervelocity fluid droplet impact. The illustration is taken from an earlier publication[9] in which the characteristic gas to solid functional expansion approach was used to ap-

proximate the initial slope of the momentum transfer and energy deposition at the surface of the target solid material. The numerical results were obtained by a direct coupling of the gas dynamic shocked phase to a full-strength Lagrangian solid phase by cyclic combination of the gas and solid dynamics using a version of the Noh[11] treatment for the gas and interface dynamics, together with Wilkin's[10] elastic-plastic solid continuum method.

The initial peak stress deposition between the solid target, water film coating, and impacting hypervelocity droplet are shown in Figure 7. With the exception of the film layer whose distribution is determined as the total impacting energy less the sum of that distributed (or predicted) in target and droplet, the initial energy deposition profiles are again developed by the model and compare well to the numerical results[9].

At this stage, the question remains, is it necessary to apply this analysis to Mach Reflection experiments?

Figure 8 shows a schematic of the cylindrical explosive driver section used to initiate an incident shock in a narrow rectangular blast wave duct at Physics International Company[7,8]*. The cylindrical wave with source at the upper left hand corner of the blast duct, impinges on the ground plane at near normal incidence for gauges located in a horizontal ground plane directly beneath the blast source. At gauges further removed from the zenith directly below the blast source, the wave reflection dynamics progress from regular to Mach reflection. A sequence of gauges located out along the horizontal ground plane gives a complete record of the history of an incident wave impinging on a horizontal surface from regular to Mach reflections[7,8].

*The assistance of the Physics International Company Staff, particularly Kerry Seifert, in supplying these data and reference 8, is gratefully acknowledged.

The next sketch, Figure 9, is used to illustrate the clean environment of the test gas obtained in the novel blast duct experiments. The explosive source of the driver is completely and perfectly separated from the test gas by an intact, collapsing plastic conical membrane which separates detonation products from the interior. Figure 10 diagrams the cylindrical wave source and the various reflection regions generated on the ground plane of the blast duct. The gauges recording the reflection signals are located left to right on the ground plane and are flush-mounted on the surface.

A diagram of the recompression gap dynamics between the rubber seal at the side of the ground plane and the vertical duct sidewall is shown in Figure 11. The expansion of shocked processed gas on reaching the sidewall gap region, followed by recompression on recirculation of the flow was the subject of a previous method-of-characteristics analysis performed by one of the writers in discussion of the experiments[7]. This primary candidate for the reproducible breakdown of the pressure signal in the regular reflection region will be discussed further in the conference.

A typical pressure time history of the ground plane sequence of pressure gauges from regular reflection at the left to Mach reflection at the right is shown in Figure 12. The pressure time history breakdown in the regular reflection region is indicated by the multiple peaks in place of the expected single sharp peak. While the gap rarefaction-compression process helped explain a reason for the breakdown in regular reflection shock structure, the amplitude of the oscillations, quantitatively overwhelmed the the analytical interpretation of the Mach reflection structure.

Figure 13 shows a correlation curve of the predicted pressure value compared with the experimental pressure value for a large number of Mach reflection duct gauge records taken at the ground plane. The black checks represent predicted reflected pressure based on non-moving rigid wall theory for the ground plane. The solid symbols are results, modified by the expansion -recompression gap consideration mentioned earlier. The open circles designate results obtained for our current yielding ground-surface model. It appears that the issue between gap recompression and surface vibrational yield is open! Surface response analysis appears to be an important component in experimental analysis of Mach reflections. Physically, the surface response of bounding container surfaces appears to be a primary candidate for serious attention in analyzing combustion cans, reactor safety vessels and the like. This is emphasized by recalling the non-linear dependence of phase rate processes and reaction processes on the density-temperature profiles and the pressures fluctuations which induce them.

III. MACH REFLECTION

Similitude

Here the discussion centers on the apparent similitude of a large number of shock tube, wedge interaction expeirments on single and double Mach reflection conducted in the Soviet Union[1,2,3]. Figures 1 and 2 are recalled to assist in the description of the dynamics of irregular Mach reflection and at least one hypothesis on the evolution of a second Mach stem incorporated in the single irregular surface reflection wave structure. Figure 14 is a plot of the results of over 30 U.S.S.R. shock tube reflection experiments. The slope of the triple point trajectory ratioed to the critical reflection angle is plotted against the wedge surface deflection angle which is also ratioed to the critical reflection angle. The cross-hatched band envelops the experimental deviation. Since these experiments embraced a large range of shock intensities from Mach Numbers of 2 to better than 8, the similarity is (at least, in the observational sense) impressively established. Furthermore, it is indicative that the gas phase non-equilibrium or caloric imprefection effects have little influence on what appears to be a fluid dynamic as opposed to thermodynamic phenomenom. Some comparisons with steady state wedge interaction phenomenom will be discussed in the conference.

Singular Perturbations

Many of the approaches in the perturbation analysis of Mach reflection have followed Lighthill[12]. The flow in the irregular reflection region

(between S and R in Figure 1) is assumed to be a small perturbation of the flow behind the incident shock, but above the reflected shock (between $(I)_1$ and R in the same figure). Conical field transformations are used to remove time from the problem, reducing the equations to stationary flow. One solves an elliptic problem for pressure [13,14,15].

An alternate procedure, followed by Ting and Ludloff[16], has some distinct advantages over these analyses. In their study, the conical flow assumption is not used. The hyperbolic equations are solved exactly in a perturbation scheme based on the usual geometric parameter (thickness ratio of wall disturbance or airfoil).

Several features of this approach have immediate appeal. First, it is satisfying that no a priori assumptions are made regarding the form of the solution. Of even greater significance to us is that solving the equations in this form exposes what seems to be the basic physical process[17] governing the transition from single to double Mach reflection.

Examination of current Soviet computations[18], together with recent experimental evidence[1,2,19] on the transition to double Mach reflection reveals a tempting physical picture of this phenomena. Namely that stagnation of a normal component of the flow behind the slip line (D) initiates compression waves which interact with the slip line forcing it to move forward in the irregular curved path sketched in Figure 1. The reflected shock (R) path adjusts to compensate for the rarefaction induced by the forward motion of the slip line. This adjustment appears as the experimentally observed "kink". Under more intense conditions, a second shock stem emanates from this point, and one obtains the double Mach configuration of Figure 2.

In their work, Ting and Ludloff[16] expand the solution to the first order correction only. They demonstrate that despite the expected absence of a significant pressure gradient at the slipstream (D) (under certain conditions), there is an appreciable density gradient. By examination of the second order corrections, we wish to demonstrate the singular character of the solutions in the neighborhood of the slip line. By a proper expansion of the solution in this domain, it is hoped that the conditions leading to the double Mach reflection will be explictly demonstrated.

IV. FUTURE DIRECTION

It is inappropriate here to initiate a list of conclusions. The study discussed here has been outlined using as its basis previous analyses and studies on related topics. Our current efforts, which have been introduced in this paper, are just commencing. For this reason, we summarize here with some notions on the indicated directions of our future studies. These will include:

- Compliant and Yielding Surface Generalization

  Here we will address the modeled response of surface dynamics subjected to momentum and concomitant energy coupling. Viscous and heat transfer processes will be incorporated.

- Wave Interaction and Reflection at Low Amplitude

  The yielding surface response is probably less important here than appropriate computational algorithms for coupling both normal and tangential flow at an arbitrarily inclined solid surface interface with the gasdynamic phase. This low amplitude, two-dimensional unsteady coupling is apparently the essential ingredient for this stage of the computational development.

- Asymptotic Analysis

  While we have just touched on this in the current paper, it is already obvious that the use of complementary analytical modeling is essential to success in characterizing the Mach Reflection flow structure and in guiding the development of numerical simulation techniques together with boundary treatment, coordinate stretching, and coordinate transformations. We are particularly committed to the use of matched

asymptotic expansions as a rational exposition technique for multiple layer fluid dynamic processes such as Mach reflection and for establishing the necessary ingredients for the numerical model.

- Computational Method Refinements

  The actual alteration of the numerical procedure, implementation of explicit or iterative indirect techniques, and development of combined procedures, are, we believe, justifiably dictated by the results of the problem analysis. This category of future direction is, thereby, left open.

V. REFERENCES

1. L.G. Gvozdeva, et. al., "Mach Reflection of Shock Waves in Real Gases", Astronautica Acta (14), pp. 503-508 (1969).

2. L.G. Gvozdeva, et. al., "Pressure and Temperature at the Wedge Surface for Mach Reflection of Strong Shock Waves", Astronautica Acta (15), pp. 503-510 (1970).

3. B.I. Zaslavskii and R.A. Safarov, "Similarity of Flows Generated During Reflection of Weak Shock Waves from a Rigid Wall and a Free Surface", (Transl.), Fizika Goreniya i Vzryva (9), 4, pp. 579-585, (1973).

4. C.P. Kentzer, "Discretization of Boundary Conditions on Moving Discontinuities", Second International Conference on Numerical Methods in Fluid Dynamics, University of California, Berkeley, California, September 15-19, (1970).

5. M.J. Abbett, "Boundary Condition Calculation Procedures for Inviscid Supersonic Flow Fields", AIAA Computational Fluid Dynamics Conference, Palm Springs, California (1973).

6. R.W. MacCormack and A.J. Paullay, "Computational Efficiency Achieved by Time Splitting of Finite Difference Operators", AIAA Paper 72-154, presented at Tenth Aerospace Sciences Meeting, San Diego, California (1972).

7. A.C. Buckingham, "Mach Reflection-Selected Analyses of the Experiments", Physics International Co., TCAM 73-13, presented at DNA Conference on HOB Effects, Washington, D.C., December (1973).

8. K. Seifert and P. Welch, "Mach Reflection Effects at High Overpressures", Physics International Co., San Leandro, California PIFR-376 (1975).

9. A.C. Buckingham and A.J. Crispino, "Computations of Hypervelocity Impact on Water Film Coated Metal", Proceedings International Conference on Computational Methods in Non-Linear Mechanics, University of Texas Press, Austin, Texas, pp. 508-516 (1974).

10. M.L. Wilkins, "Calculations of Elastic-Plastic Flow", Methods In Computational Physics (3), Academic Press, N.Y., pp. 211-263 (1964).

11. W.F. Noh, "CEL: Coupled Eulerian-Lagrange Code", Methods In Computational Physics, (3), Academic Press, N.Y., pp. 117-179 (1964).

12. Lighthill, M.J., "The Diffraction of Blast, I", Proc. Roy. Soc. A, (198), pp. 454-470 (1949).

13. Chester, W., "The Diffraction and Reflection of Shock Waves", Quart. J. Mech. Appl. Math, (7), pp. 57-82 (1954).

14. Smyrl, J.L., "The Impact of a Shock Wave on a Thin Two-Dimensional Aerofoil Moving at Supersonic Speed", J. Fluid Mechanics, (15), pp. 223-241 (1963).

15. Blakenship, V.D., "Shock-Shock Interaction on a Slender Supersonic Cone", J. Fluid Mechanics, (22) 39, pp. 599-615 (1965).

16. Ting, L. and Ludloff, H.F., "Aerodynamics of Blasts", J. Aeronautical Sciences, (19), pp. 317-328 (May, 1952).

17. Bleakney, W. and Taub, A.H., "Interaction of Shock Waves" Reviews of Modern Physics, (21), 4, pp. 584-605 (1949).

18. Lipnitskii, Y.M. and Lyakhov, V.N., "Numerical Solution of the Problem of Shock-Wave Diffraction on a Wedge", Mekhanika Znidkosti i Gaza, (6), pp. 88-93 (1974).

19. Merritt, D.L., "Mach Reflection on a Cone", AIAA Journal, (6), 6, pp. 1208-1209 (1968).

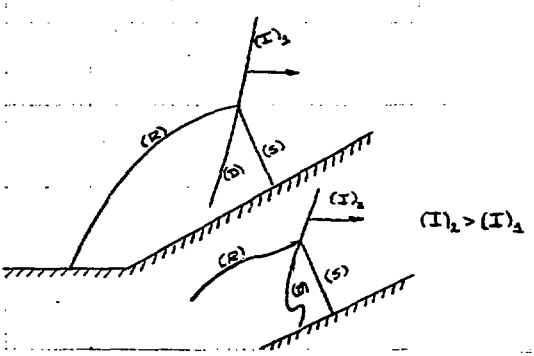

FIGURE 1. CONCEPTUAL SINGLE MACH REFLECTION-INTENSIFICATION LEADING TO DOUBLE MACH REFLECTION.

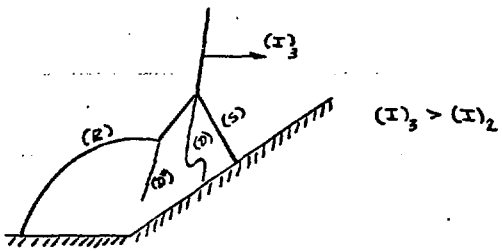

FIGURE 2. CONCEPTUAL FULLY DEVELOPED DOUBLE MACH REFLECTION.

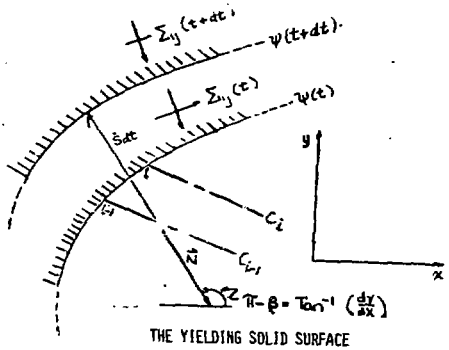

THE YIELDING SOLID SURFACE

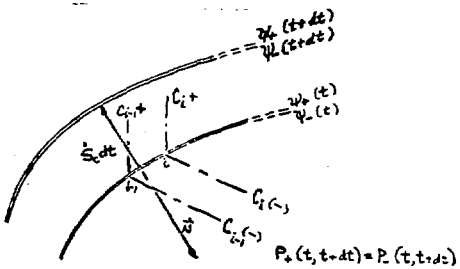

MOTION OF GASDYNAMIC INTERFACE

FIGURE 3. CONCEPTUAL MATCHING OF WAVE AND STREAM SURFACES.

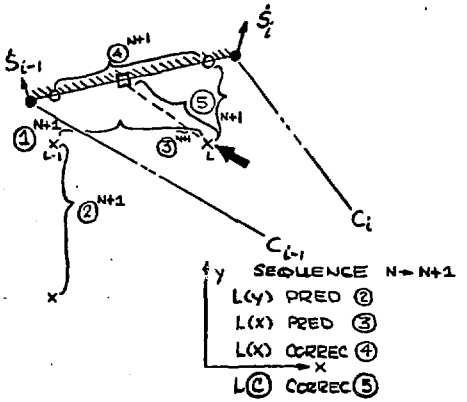

② STANDARD L(Y) PREDICTOR

③ STANDARD L(X) PREDICTOR

④ NON-STANDARD L(X) "CORRECTOR" INTEGRATION OF CHARACTERISTIC B.C. EQNS. (11), (12), (13), (14).

⑤ NON-STANDARD SIMPLE WAVE CORRECTOR EQN. (15).

FIGURE 4. CALCULATION AT THE SOLID MOVING SURFACE.

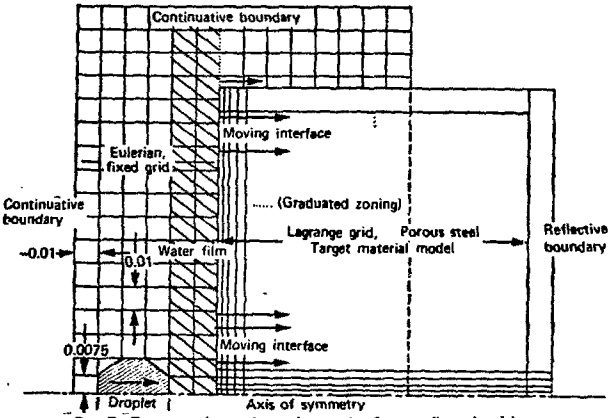

FIG. 5 Representative zoning and geometry for two-dimensional impact.

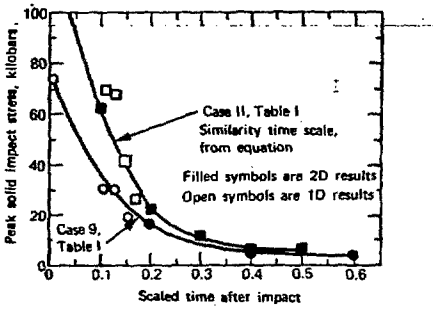

Fig. 6. Peak stress versus time.

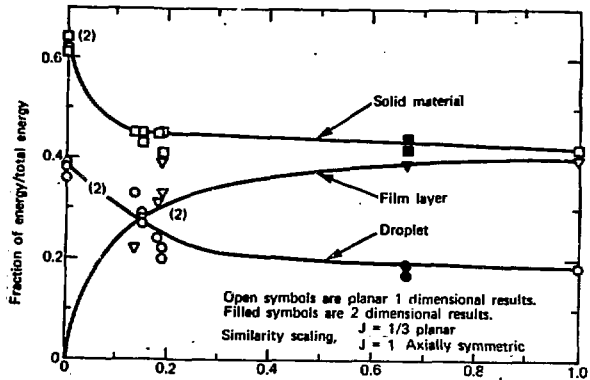

Fig 7. Energy partition as a function of relative film thickness.

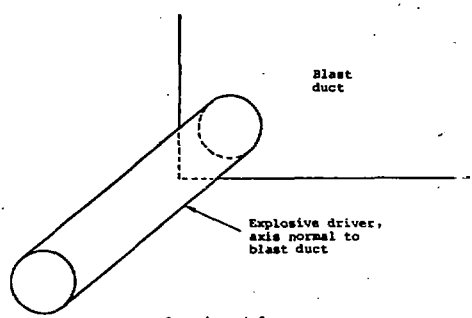

a. Overview, t=0

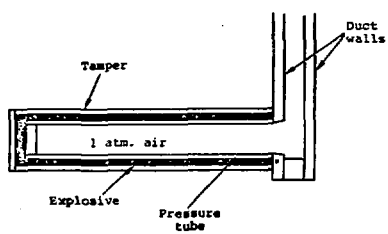

b. Side view, t=0

Fig 8. Schematic of reflected driver operation.

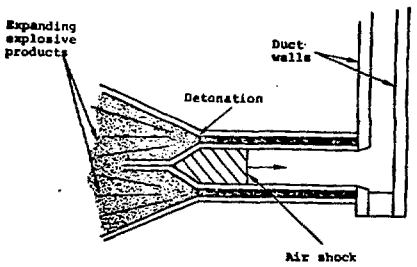

c. Side view, $t=t' > 0$

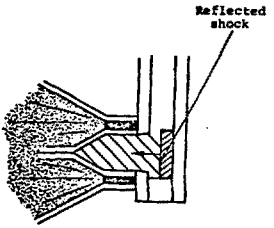

d. Side view, $t=t'' > t'$

Fig. 9 Schematic of reflected driver operation.

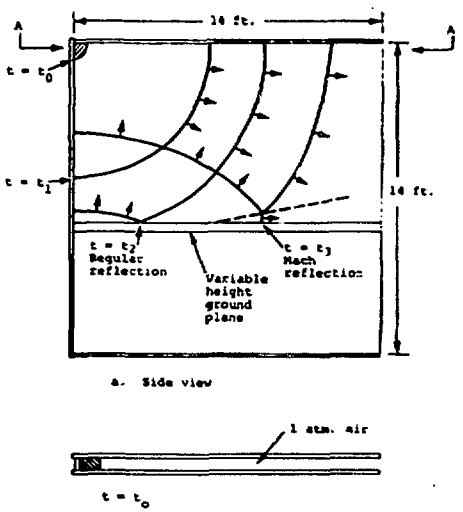

Fig. 10 Schematic of blast duct operation.

Fig. 11.
GEOMETRY OF BLAST DEFLECTOR SIDEWALL
GROUND PLANE EDGE GAP REFLECTION

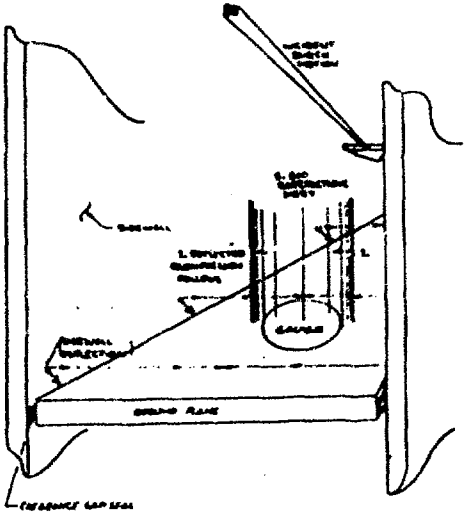

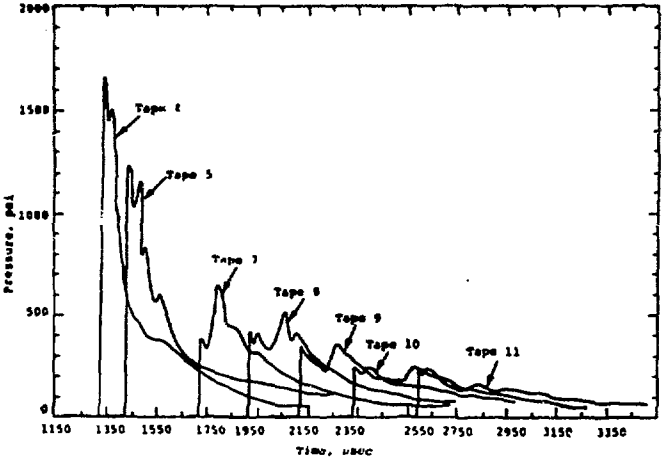

Fig 12. *Pressure-time histories of Shot HR-205.*

FIGURE 13. EXPERIMENTAL VS. PREDICTED REFLECTED PRESSURE, MR DUCT

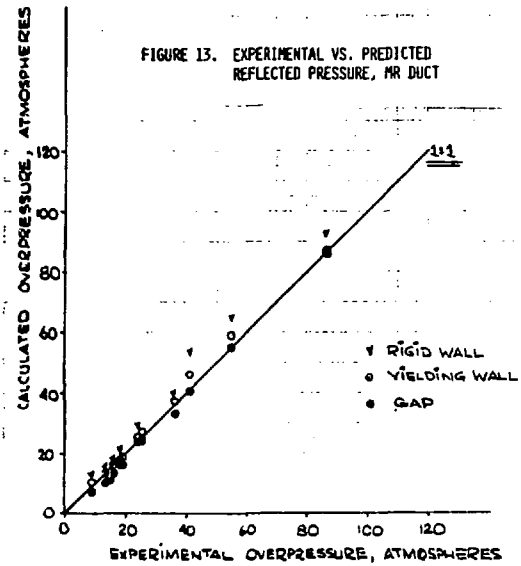

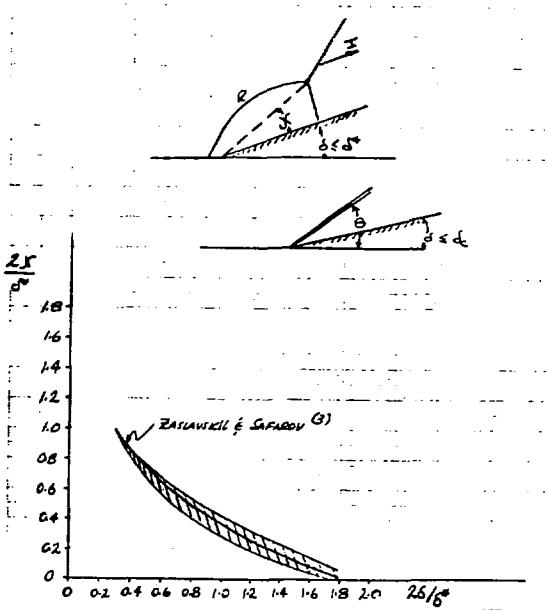

FIGURE 14. FLOW DEVIATION SIMILARITY IN MACH REFLECTION